Results of a VSP experiment at the Resurgent Dome, Long Valley caldera, California

Roland Gritto,[1] Arturo E. Romero,[2] and Thomas M. Daley[1]

[1] A vertical seismic profiling experiment has been conducted at the DOE well LVF 51–20 at the resurgent dome at Long Valley caldera, California. The current paper is intended to report the velocity results derived from this experiment to seismically constrain the area around the resurgent dome. We report the results of velocity logs, V_p/V_s ratios, and V_pV_s products for the depth interval from 880–1980 m. The Bishop tuff can be divided into three zones (top-to-bottom) of intermediate velocities ($V_p \approx 4.0$ km/s, $V_s \approx 2.3$ km/s), followed by higher velocities ($V_p = 4.7$ km/s, $V_s = 2.9$ km/s) in the lower-central part, and a decrease back to the lower values at the bottom of the sequence. The analysis of V_pV_s data suggested a decrease in porosity in the lower-central section of the tuff as a possible explanation, which was supported by direct density measurements from a nearby location.   INDEX TERMS: 7203 Seismology: Body wave propagation; 7205 Seismology: Continental crust (1242); 7280 Seismology: Volcano seismology (8419). **Citation:** Gritto, R., A. E. Romero, and T. M. Daley (2004), Results of a VSP experiment at the Resurgent Dome, Long Valley caldera, California, *Geophys. Res. Lett.*, *31*, L06603, doi:10.1029/2004GL019451.

1. Introduction

[2] The Long Valley caldera (LVC) is a Quaternary volcanic structure, located at the intersection of the Sierra Nevada frontal fault escarpment and the western margin of the Basin and Range tectonic province. A map view of the LVC region is presented in Figure 1.

[3] In 1980, strong evidence of renewed magma movement became apparent following a series of large magnitude earthquake sequences accompanied by rapid surface uplift. While several geophysical studies suggest the existence of a magma chamber beneath the resurgent dome [i.e., *Hill*, 1976], other investigations do not support the presence of a sizable magma body at shallow to mid-crustal depth beneath LVC [*Kissling*, 1988]. The latter study relates the encountered lower mid-crustal velocities to hydrothermal alteration and/or extensive fractures.

[4] Most of the seismological studies were performed as surface refraction experiments [*Hill et al.*, 1985], facing the difficulties of two-way wave propagation through the highly attenuative non-welded tuff and interpretations of the reflected seismic energy with little knowledge about the actual subsurface velocities.

[5] In an attempt to determine a better velocity model, among other goals, the Lawrence Berkeley National Laboratory (LBNL) conducted a vertical seismic profiling (VSP) experiment within LVC under the Department of Energy's Basic Energy Science and Continental Scientific Drilling program. The experiment was conducted at the Long Valley Federal 51–20 well (LVF 51–20, also referred to as LVEW) after completion of the second drilling phase and is the only deep VSP performed at LVC to date. The location of the well lies within the center of the resurgent dome (Figure 1). The borehole measurements have the advantage of improved signal-to-noise ratio, because of the quieter environment and because of one-way wave propagation through the highly attenuating surface layers. The current paper is intended to report the results of the velocity analysis, including velocity ratio (V_p/V_s) and velocity product (V_pV_s), to provide local velocity constrains within the resurgent dome for future seismic studies of LVC.

2. Data Acquisition and Processing

[6] The seismic source of the VSP experiment was a P-vibroseis truck, located 165 m from the well, exciting sweeps 12 seconds long with frequency content of 10 Hz to 58 Hz. The data were acquired with a sample rate of 2 ms between 550 m and 2072 m depth at 15 m intervals. Shallower data acquisition was prevented by multiple borehole casing, which degraded data quality. The receiver was a three-component, high-temperature, hydraulic wall-locking borehole seismometer. The corner frequency of the geophones was 14 Hz with a flat response up to 500 Hz.

[7] Data processing consisted of noise editing, trace stacking to improve the signal-to-noise ratio, and correlating the traces with the source sweep. Strong P-to-S-wave conversions in the shallow subsurface produced sufficient S-wave arrivals on the seismograms, such that P- and S-wave data could be analyzed.

[8] A numerical rotation of the geophone components was applied to maximize the depth coherence of P- and S-waves [*Daley et al.*, 1988]. The rotated data are presented in Figure 2, separated into radial and transverse components. The quality of the shallowest traces is adversely effected by scatter and ringing in the waveforms, caused by problems with the cement bond of the well casing. Therefore, the following velocity analysis will be performed over a depth interval from 880–1980 m and 980–1980 m for P- and S-waves, respectively.

3. Analysis of Velocity, V_p/V_s, and V_pV_s Logs

[9] The data processing was followed by the determination of the first arrival times for the direct P- and S-waves. Assuming straight ray geometry between the source and receiver positions in the well, interval velocities for every

[1]Center for Computational Seismology, Earth Sciences Division, Lawrence Berkeley National Laboratory, Berkeley, California, USA.
[2]Exxon Production Research Company, Houston, Texas, USA.
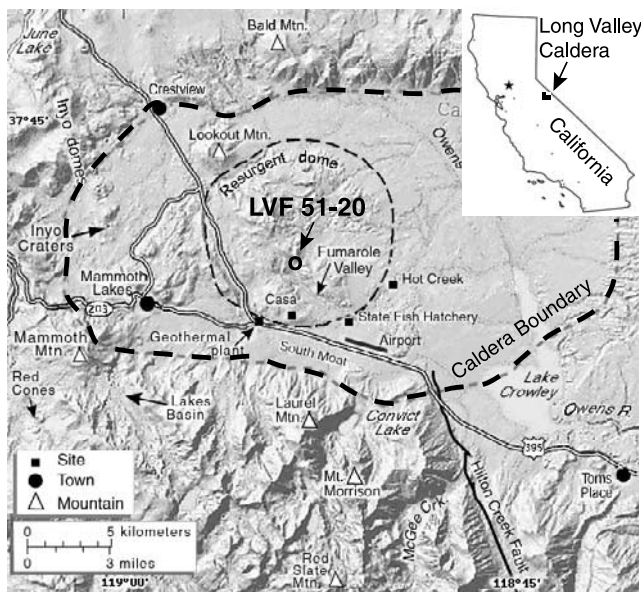
Figure 1. Map of Long Valley region adopted from USGS. The location of LVF 51–20 is indicated by the circle inside the resurgent dome.

receiver location were computed. The arrival times were determined by cross-correlation technique yielding sub-sample accuracy. This was achieved by first cross-correlating the traces one sample at a time, followed by taking their ratio in the frequency domain and determining the slope of the resulting phase spectrum at low frequencies [*Nadeau et al.*, 1994]. The slope was then added to the shift determined in the time domain to gain subsample accuracy. Because some scatter remained in the resulting velocities estimates, they were subsequently averaged over a 10-point running window of 150 m length that was comparable to the dominant compressional- and shear wavelength of λ_p = 160 m and λ_s = 125 m, respectively. The estimated uncertainty of the arrival times is ±1 ms for P-waves and ±3 ms for S-waves over the 10-point average. These uncertainties were subsequently converted to upper and lower bounds for the velocity estimates.

3.1. P- and S-Wave Velocities

[10] The velocity-depth estimates are shown in the left panel of Figure 3. Within the Bishop tuff, the velocity profiles can be subdivided into three sections as indicated by the dashed horizontal lines. The upper and lower zones reveal intermediate velocities (V_p = 3.5–4.5 km/s, V_s = 2.0–2.7 km/s), while the central section reveals higher velocity values (V_p = 4.7 km/s, V_s = 2.9 km/s). At the bottom of the tuff, the transition to metavolcanics and the underlying metasediments is reflected by an increase in P- and S-wave velocities to $V_p \geq 5.0$ km/s and $V_s \geq 3.0$ km/s, respectively. Previous seismic studies in this area produced similar results. [*Romero et al.*, 1993] conducted V_p and V_s tomography studies using local earthquake travel time data, and reported, for the area around the current VSP well, velocity estimates of V_p = 2.7 km/s at 0 km depth and V_p = 5.4 km/s at 2 km depth. Interpolation between these estimates would yield value of V_p = 4.05 km/s at 1 km depth. Similarly, the reported S-wave velocity estimates are V_s = 1.7 km/s at 0 km depth, V_s = 3.0 km/s at 2 km depth, and an interpolated value
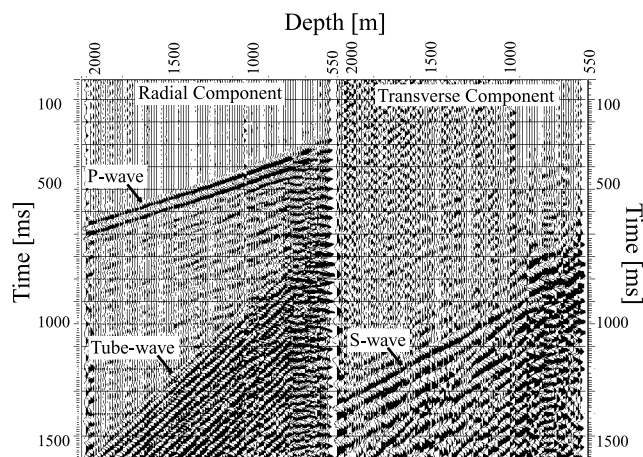
Figure 2. Seismic data after correlation and rotation into the wavefront coordinate system. In the new coordinate system, the components correspond to radial and transverse components. The upper 16 traces show strong reverberations in the wave forms caused by problems with the cement bond of the well casing.

of V_s = 2.35 km/s at 1 km depth. These values are well in accordance with the velocity estimates reported in the present study. In addition, [*Hill et al.*, 1985] conducted seismic P-wave refraction studies across the resurgent dome and reported velocity estimates of V_p = 3.9–4.1 km/s at 1 km depth and V_p = 4.9–5.2 km/s at 2 km depth, which again agrees with the present findings. The depth distribution of alteration minerals, presented in the right column in Figure 3, shows an even distribution of minerals throughout the tuff
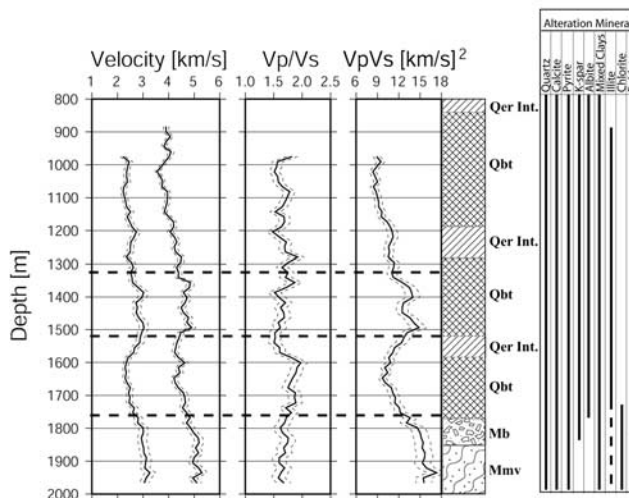
Figure 3. Velocity, velocity-ratio, and velocity-product logs for the DOE exploratory well LVF 51–20. The upper and lower bounds are indicated by the thin dashed lines. The dashed horizontal lines are intended to divide the velocity logs into sections of similar velocities (see text). The stratigraphic and mineralogic columns, reproduced from *McConnell et al.* [1995], are based on data from core analyses and televiewer information. Qer: Postcaldera volcanics (rhyolite, vesicular pumice, welded tuff); Qbt: Bishop tuff; Qer Int.: dike intrusions (rhyolite); Mb: mixed breccia; Mmv: Mesozoic metavolcanics.

section, which precludes the mineralogy as the leading cause for the velocity variations. The transition to metavolcanic rocks at the base of tuff, however, is characterized by an increase in both P- and S-wave velocity, which is caused by a change in mineralization, primarily the presence of Chlorite and Epidote, with velocities of $V_p = 6.75-7.1$ km/s for the former and $V_p = 6.43$ km/s and $V_s = 4.2$ km/s for the latter [*Carmichael*, 1982]. The velocity distribution within the Bishop tuff is caused by the depositional and cooling history of tuffs, which produces significant variations in density and porosity, as we will address in a later section.

3.2. V_p/V_s-Ratio

[11] The interpretation of seismic velocity logs is non-unique, because many rocks with different physical states have similar seismic velocities. Factors such as fracturing, pore pressure, fluid saturation, and partial melt affect seismic velocities. Therefore, it is useful to consider velocity ratios to differentiate between the different physical effects in the medium. *Moos and Zoback* [1983] show that fluid saturated fractures decrease both V_p- and V_s-velocities, while it increases the V_p/V_s-ratio. *Dvorkin et al.* [1999] demonstrated that for water saturated rocks V_p/V_s values increase with increasing pore pressure (i.e., differential pressure decreases), while for dry rocks V_p/V_s values decrease with increasing pore pressure. *Sanders et al.* [1995] investigate V_p/V_s-ratios from seismological observations at LVC and conclude that high values suggest the existence of high temperatures and perhaps partial melt or an increase in fracture concentration in saturated rocks. Low V_p/V_s-ratios, in contrast, are consistent with supercritical fluids and the presence of gas phases.

[12] The V_p/V_s-ratio, derived from the velocity measurements, is shown in the central panel in Figure 3. The average value over the depth interval of 1.69 ± 0.09 is slightly lower than the crustal average of 1.73. The upper and middle zones of the Bishop tuff from 900–1520 m show only small variations in V_p/V_s-ratio, while the P- and S-wave velocities increase simultaneously. In the lower section of the tuff (1520–1750 m), however, the V_p/V_s-ratio increases, which is caused by the stronger decrease in S-wave velocity relative to the P-wave velocity over the same depth interval. Partial melt is unlikely the cause for the high ratio, because the temperature profile in the borehole, shown in Figure 4, does not reveal an increased temperature gradient for this depth interval. Furthermore, the shaded region of the temperature profile, representing the depth interval of the velocity estimates, shows an almost constant gradient of 30°C/1000 m throughout the Bishop tuff, while the values at the bottom of the profile indicate a slightly higher gradient within the basement rocks. In contrast, the temperature increases at 550 and 750 m depth are likely associated with zones of lateral hydrothermal fluid flow delineated by *Sorey et al.* [1991]. In the absence of temperature anomalies around the well, the likely cause for the V_p/V_s high is a fluid saturated zone of high porosity or fracture concentration. Similar observations were reported by *Lees and Wu* [2000] for fluid saturated production zones at the Coso geothermal field, California.

3.3. $V_p V_s$-Product

[13] The $V_p V_s$-product of seismic velocities has been used to determine porosity in volcanic settings, where it was
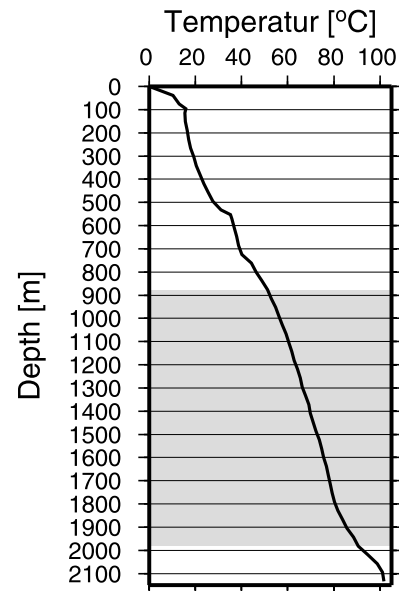
Figure 4. Temperature log of LVF 51–20. The grey shaded area indicates the depth range of the current velocity analysis.

observed that $V_p V_s$ decreases with increasing porosity [*Lees and Wu*, 2000]. The estimation of $V_p V_s$-values is particularly useful in geothermal areas, where the understanding of fluid flow depends more on porosity than lithological settings. In the following section we attempt to relate $V_p V_s$ to the porosity profile of the Bishop tuff.

[14] The $V_p V_s$-product is displayed in the right panel in Figure 3. The trend of $V_p V_s$ increases in the top half of the depth section, peaking in the lower-central part, before it decreases again towards the base of the tuff sequence. The increase below 1650 m is caused by higher velocity values in the underlying basement rocks that are mapped in the tuff by the length of the smoothing window (150 m). The trend of the $V_p V_s$-values suggests higher porosity values at the top and base of the tuff, while the center appears more dense. To investigate this possibility a density profile of the Bishop tuff was plotted in the left column of Figure 5. The density data was measured on exposed sections of the Bishop tuff in Owens Gorge outside the boundary of LVC about 20 km south-east of VSP well [*Ragan and Sheridan*, 1972]. Therefore, the thickness of the tuff in Figure 5 is reduced relative to its thickness at the location of the VSP well near the center of the eruption within LVC. Nevertheless, the cooling history of the tuff is very similar in both locations, such that the general trend of the data in Figure 5 can be used as an analog for the tuff layer in the vicinity of the VSP well. In order to estimate porosity from the density profile, we use the bulk density ρ_b of a fully water saturated rock, with porosity ϕ, matrix density ρ_m, and water density ρ_w as given by

$$\rho_b = (1 - \phi)\rho_m + \phi\rho_w. \quad (1)$$

Using this equation the proposity ϕ can be expressed as

$$\phi = (\rho_b - \rho_m)/(\rho_w - \rho_m). \quad (2)$$

Based on this equation, the density values in Figure 5 can be converted to porosity using the density of water and the
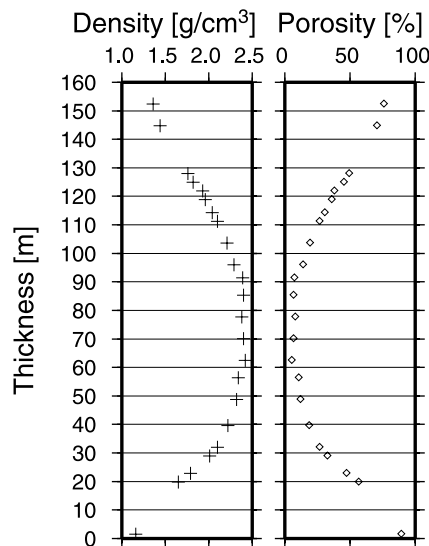
Figure 5. Density and porosity depth profile for the Bishop tuff at Owens Gorge, California. The density profile was measured by [*Ragan and Sheridan*, 1972], while the porosity profile was calculated using equation (2) and the density profile (see text).

matrix as $\rho_w = 1.0$ g/cm^3 and $\rho_m = 2.5$ g/cm^3, respectively. The value for the matrix density was chosen to represent the grain density of tuff. The resulting porosity profile in Figure 5 mimics the reverse trend of the V_pV_s in Figure 3. The lower-central section of the tuff sequence shows the lowest porosity with values of $\approx 5\%$. The density/porosity profile was created by different cooling regimes within the tuff. The top and bottom cooled fastest after the initial eruption, such that welding could not take effect as efficiently as in the central section of the tuff layer, which created a more compact layer. The reason for the displacement of the low porosity/high density zone below the center of the tuff flow may be explained by faster cooling rates from the top [*Ragan and Sheridan*, 1972].

[15] The increase in V_pV_s in Figure 3 correlates well with the presence of the metavolcanics at the bottom of the profile, suggesting an additional reduction in porosity relative to the Bishop tuff.

4. Conclusion

[16] The intention of this paper was to report the velocity estimates obtained during the VSP experiment at LVF 51–20, to better constrain the velocity model in the vicinity of the resurgent dome for future seismic investigations. The acquired data yielded P- and S-wave velocity results between 880–1980 m and 980–1980 m, respectively. The determination of V_p/V_s and V_pV_s from the velocities helped to constrain the interpretation of the data. Nevertheless, a more thorough investigation of the results could quantify the interpretation of the data in the vicinity of the well by reproducing the observed seismic data through numerical modeling using all available physical parameters. However, such investigations are beyond the intended scope of this paper.

[17] The available temperature log did not indicate the presence of an anomalous temperature zone in the vicinity of the well between 900 and 2000 m depth. The combination of velocity- and V_pV_s-logs suggested a region of decreased porosity throughout the lower-central densely-welded part of the Bishop tuff with higher porosity estimates above and below. These findings correlate well with density measurements of the tuff from locations along the boundary of LVC. The lower section of the Bishop tuff may be additionally fractured as indicated by an increase in V_p/V_s. The metavolcanics at the base of the survey are represented by an increase in both P- and S-wave velocities and a further reduction in density. The current analysis indicated a degree of heterogeneity throughout the Bishop tuff, similar to that of ash flows in other areas, which warrants further studies of the physical parameters to obtain a better understanding of the eruption processes and the depositional history of LVC.

References

Carmichael, R. S. (1982), *Handbook of Physical Properties of Rocks*, CRC Press, Boca Raton, Fla.

Daley, T. M., T. V. McEvilly, and E. L. Majer (1988), Analysis of P- and S-wave vertical seismic profile data from the Salton Sea scientific drilling project, *J. Geophys. Res.*, *93*, 11,025–11,036.

Dvorkin, J., G. Mavko, and A. Nur (1999), Overpressure detection from compressional- and shear-wave data, *Geophys. Res. Lett.*, *26*, 3417–3420.

Hill, D. P. (1976), Structure of Long Valley caldera from seismic refraction experiments, *J. Geophys. Res.*, *81*, 745–753.

Hill, D. P., R. A. Bailey, and A. S. Ryall (1985), Active tectonic and magmatic processes beneath Long Valley caldera, eastern California: An overview, *J. Geophys. Res.*, *90*, 11,111–11,120.

Kissling, E. (1988), Geotomography with local earthquake data, *Rev. Geophys.*, *26*, 659–698.

Lees, J. M., and H. Wu (2000), Poisson's ratio and porosity at Coso geothermal area, California, *J. Volcanol. Geotherm. Res.*, *95*, 157–173.

McConnell, V. S., C. K. Shearer, J. C. Eichelberger, M. J. Keskin, P. W. Layer, and J. J. Papike (1995), Rhyolite intrusions in the intracaldera Bishop tuff, Long Valley caldera, California, *J. Volcanol. Geotherm. Res.*, *67*, 41–60.

Moos, D., and M. D. Zoback (1983), In situ studies of velocity in fractured crystalline rocks, *J. Geophys. Res.*, *88*, 2345–2358.

Nadeau, R. M., M. Antolik, P. A. Johnson, W. Foxall, and T. V. McEvilly (1994), Seismological Studies at Parkfield III: Microearthquake clusters in the study of fault-zone dynamics, *Bull. Seismol. Soc. Am.*, *84*, 247–263.

Ragan, D. M., and M. F. Sheridan (1972), Compaction of the Bishop Tuff, California, *Geol. Soc. Am. Bull.*, *83*, 95–106.

Romero, A. E., T. V. McEvilly, E. L. Majer, and A. Michelini (1993), Velocity structure of the Long Valley caldera from the inversion of local earthquake P and S travel times, *J. Geophys. Res.*, *98*, 19,869–19,879.

Sanders, C. O., S. C. Ponko, L. D. Nixon, and E. A. Schwartz (1995), Seismological evidence for magmatic and hydrothermal structure in Long Valley caldera from local earthquake attenuation and velocity tomography, *J. Geophys. Res.*, *100*, 8311–8326.

Sorey, M. L., G. A. Suemnicht, N. C. Sturchio, and G. A. Nordquist (1991), New evidence on the geothermal system in Long Valley, California, from wells, fluid sampling, electrical geophysics, and age determinations of hot-spring deposits, *J. Volcanol. Geotherm. Res.*, *48*, 229–263.

———————————

T. M. Daley and R. Gritto, Center for Computational Seismology, Earth Sciences Division, Lawrence Berkeley National Laboratory, One Cyclotron Road, Berkeley, CA 94720, USA. (tmdaley@lbl.gov; rgritto@lbl.gov)

A. E. Romero, Exxon Production Research Company, Houston, TX 77252, USA. (aeromer@exxon.com)